

# The rotational broadening of V395 Carinae. Implications on the compact object's mass<sup>★</sup>

T. Shahbaz<sup>1</sup> and C. A. Watson<sup>2</sup>

<sup>1</sup> Instituto de Astrofísica de Canarias, c/ via Lactea s/n, La Laguna, 38200 Tenerife, Spain  
e-mail: tsh@iac.es

<sup>2</sup> Department of Physics and Astronomy, University of Sheffield, Hicks Building, Sheffield S3 7RH, UK  
e-mail: c.watson@sheffield.ac.uk

Received 10 July 2007 / Accepted 8 August 2007

## ABSTRACT

**Context.** The masses previously obtained for the X-ray binary 2S 0921–630 inferred a compact object that was either a high-mass neutron star or low-mass black-hole, but used a previously published value for the rotational broadening ( $v \sin i$ ) with large uncertainties.

**Aims.** We aim to determine an accurate mass for the compact object through an improved measurement of the secondary star's projected equatorial rotational velocity.

**Methods.** We have used UVES echelle spectroscopy to determine the  $v \sin i$  of the secondary star (V395 Car) in the low-mass X-ray binary 2S 0921–630 by comparison to an artificially broadened spectral-type template star. In addition, we have also measured  $v \sin i$  from a single high signal-to-noise ratio absorption line profile calculated using the method of Least-Squares Deconvolution (LSD).

**Results.** We determine  $v \sin i$  to lie between  $31.3 \pm 0.5 \text{ km s}^{-1}$  to  $34.7 \pm 0.5 \text{ km s}^{-1}$  (assuming zero and continuum limb darkening, respectively) in disagreement with previous results based on intermediate resolution spectroscopy obtained with the 3.6 m NTT. Using our revised  $v \sin i$  value in combination with the secondary star's radial velocity gives a binary mass ratio of  $0.281 \pm 0.034$ . Furthermore, assuming a binary inclination angle of  $75^\circ$  gives a compact object mass of  $1.37 \pm 0.13 M_\odot$ .

**Conclusions.** We find that using relatively low-resolution spectroscopy can result in systemic uncertainties in the measured  $v \sin i$  values obtained using standard methods. We suggest the use of LSD as a secondary, reliable check of the results as LSD allows one to directly discern the shape of the absorption line profile. In the light of the new  $v \sin i$  measurement, we have revised down the compact object's mass, such that it is now compatible with a canonical neutron star mass.

**Key words.** stars: neutron – stars: individual: V395 Car (=2S 0921–630) – X-ray: binaries – stars: binaries: close

## 1. Introduction

2S0921–630 was identified with a  $\sim 16$  mag blue star (Li et al. 1978), V395 Car, whose optical spectrum was characteristic of a low-mass X-ray binary (Branduardi-Raymont et al. 1983). The secondary star is thought to be a halo object in orbit with a K0 III companion star; absorption lines of the companion have been detected (Branduardi-Raymont et al. 1983; Shahbaz et al. 1999; Shahbaz et al. 2004; Jonker et al. 2005). Indeed V395 Car is one of those rare low-mass X-ray binaries in which the secondary is visible despite the presence of a luminous disk. The inclination angle of V395 Car is relatively well constrained and must be high since partial eclipses of the compact object and accretion disc (typical for accretion-disc corona sources) have been observed at both X-ray and optical wavelengths (e.g. Branduardi-Raymont et al. 1983; Chevalier & Ilovaisky 1981; Mason et al. 1987). There has been no detection of type I X-ray bursts of pulsations, so the nature of the compact object is unclear.

Intermediate-resolution optical spectroscopy revealed the donor to be a K0 III star with a rotational velocity of  $v \sin i = 64 \pm 9 \text{ km s}^{-1}$ , contributing 25% to the observed flux near H $\alpha$  (Shahbaz et al. 1999). Further optical spectroscopy yielded the

**Table 1.** Log of observations. The orbital ephemeris was taken from Shahbaz et al. (2004).

Object	UT Date	UTC	Orbital phase
V395 Car	13/04/06	23:47:06	0.19
V395 Car	22/04/06	01:23:09	0.08
V395 Car	10/05/06	00:20:52	0.08
HD83155	10/05/06	01:05:56	–

the orbital period (9.0035 d) and the secondary star's radial velocity which, when combined with the  $v \sin i$  measurements (with rather large uncertainties), led to the conclusion that the system contains either a massive neutron star or a low-mass black hole (Shahbaz et al. 2004; Jonker et al. 2005). In this paper we present the results of UVES echelle spectroscopy aimed at refining the  $v \sin i$  measurement, which is essential for an accurate determine of the binary masses.

## 2. Observations and data reduction

We obtained spectra of V395 Car in service mode with the UV-Visual Echelle Spectrograph (UVES) at the European Southern Observatory (ESO) Observatorio Cerro Paranal, using the 8.2 m

<sup>★</sup> Based on observations collected at the European Southern Observatory, Chile, under the programme 077.D-0579A.

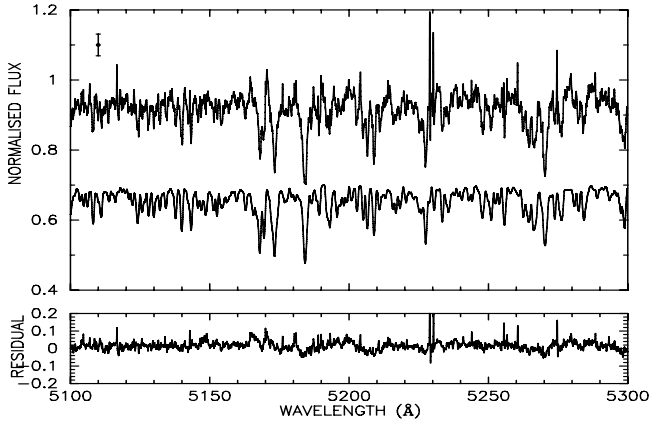


**Fig. 1.** The small section of the green spectra of V395 Car. In the *upper panel* the top spectrum is the V395 Car and the bottom spectrum is the K0 III template star rotationally broadened by  $34.7 \text{ km s}^{-1}$  using a continuum limb-darkened spherical rotation profile and scaled to match the top spectrum. The error bars show the typical uncertainties. There are a number of resolved lines in the V395 Car spectrum that are well matched by the K-star. The *bottom panel* shows the residual spectrum after the optimal subtraction.

Very Large Telescope (VLT). A log of observations is given in Table 1. The UVES standard dichroic DIC1 was used yielding spectra covering the spectral ranges 3800–4500 Å (blue), 4800–5800 Å (green) and 5800–6800 Å (red). The blue spectrum is recorded with a single CCD detector, while the red arm is covered by a mosaic of two CCD chips, leading to a small gap in the red spectrum. Three spectra of V395 Car were taken using an exposure time of 2400 s and a K0 III spectral type template star (HD 83155) was also observed. An 0.8 arcsec slit was used resulting in a resolving power of 43 000 and an instrumental velocity resolution of  $6.4 \text{ km s}^{-1}$  (*FWHM*). We used the UVES pipeline software which provides an absolute flux calibrated spectrum. The procedure consisted of bias subtraction, flat-fielding, wavelength calibration using ThAr lamps and absolute flux calibration.

### 3. The rotational broadening

We normalized the individual V395 Car and template star flux calibrated spectra by dividing by a first-order polynomial fit, and then subtracting a high-order spline fit to carefully selected continuum regions. This ensures that line strength is preserved along the spectrum and is particularly important when the absorption lines are veiled by differing amounts over a wide wavelength range. The individual spectra were then corrected for radial velocity shifts, determined by cross correlating the individual V395 Car spectra with the template K0 III star (using regions devoid of emission and interstellar lines), and then combined in order to improve the signal-to-noise ratio. The V395 Car and template star spectra were then binned on the same uniform velocity scale. The final blue spectrum of V395 Car had a signal-to-noise ratio of 15 in the continuum, whereas the green and red spectra of V395 Car had a signal-to-noise ratio of 35 in the continuum (see Fig. 1). A zoom of the significant emission line features is shown in Fig. 2.

The spectra of V395 Car were taken near orbital phase 0.0 (inferior conjunction of the secondary star) when the secondary star’s contribution to the observed flux is at its most. Although, the smearing of the spectral lines associated with the radial velocity of the secondary star during its orbital motion is also at its

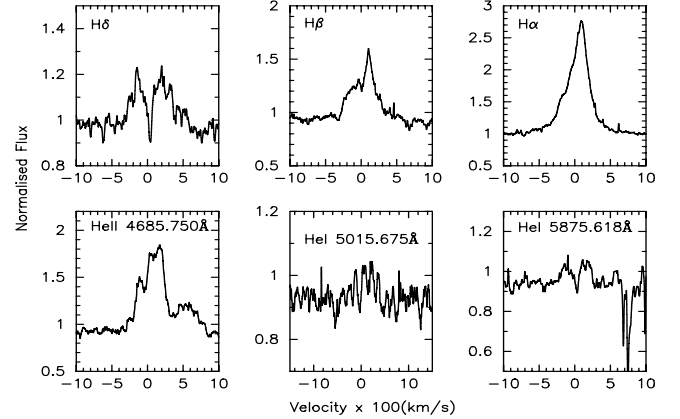


**Fig. 2.** Zooms of the most prominent emission line features.

maximum, the relatively short exposures (2400 s) compared to the long orbital period results in a maximum orbital smearing of only  $1.8 \text{ km s}^{-1}$ .

The secondary star’s rotational broadening combined with the radial velocity semi-amplitude is essential for determining the binary mass ratio. In principle one would determine the mass ratio directly by comparing the secondary star’s spectrum with a model spectrum of a Roche-lobe filling secondary star, (Shahbaz 2003). However, this requires an extremely high quality data ( $S/N > 150$ ), which our data do not have. Therefore in order to determine the rotational broadening of the secondary star  $v \sin i$  we follow the standard procedure described by Marsh et al. (1994). We subtracted a constant (representing the fraction of light from the template star) multiplied by a rotationally broadened version of the template star. The optimal subtraction routine adjusts the constant, minimizing the residual scatter ( $\chi^2$ ) between the spectra. We broadened the template star spectrum from 10 to  $90 \text{ km s}^{-1}$  in steps of  $0.2 \text{ km s}^{-1}$  using a spherical rotation profile (Gray 1992) with a linear limb-darkening coefficient appropriate for a K0 III star at the central wavelengths of the green and red spectra. The analysis was carried on the green and red spectra only, because of the poor signal-to-noise in the blue spectrum. The regions used in the analysis excluding the H I and He I emission line regions and interstellar features Na I 5899.95, 5895.92 Å and 6284 Å. The additive nature of the  $\chi^2$  distribution allows us to add the  $\chi^2$  distribution for the green and red spectra, which is the same as performing the  $v \sin i$  analysis using the combined green and red spectra. We obtained a minimum reduced  $\chi^2$  of 0.97 corresponding to a  $v \sin i$  of  $34.5 \pm 0.3 \text{ km s}^{-1}$  (see Fig. 3). Similar results have also been recently obtained by Steeghs & Jonker (2007).

It should be noted that the analysis above assumes that the limb-darkening coefficient appropriate for the radiation in the lines is the same as for the continuum. However, in reality this is not the case, and the absorption lines in late-type stars will have core limb-darkening coefficients much smaller than that appropriate for the continuum (Collin & Truax 1995). In order to determine the extreme limits for  $v \sin i$  we also repeated the above analysis using zero limb-darkening and obtained a  $v \sin i$  of  $31.4 \pm 0.2 \text{ km s}^{-1}$ . As one can see, the main uncertainty in the  $v \sin i$  determination comes from the uncertain limb-darkening coefficient.

What is clearly evident is that the rotational broadening determined using UVES spectra is much lower compared to the rotational broadening of  $64 \pm 9 \text{ km s}^{-1}$  obtained previously using

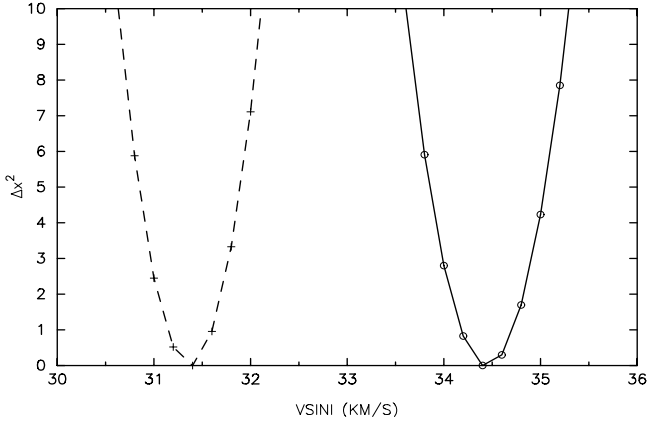


**Fig. 3.** The results of the  $v \sin i$  analysis using the green and red spectra. The variation of  $v \sin i$  with  $\chi^2$  is shown for the continuum limb-darkening (solid line) and the zero limb-darkening (dashed line) case.

New Technology Telescope (NTT) data (Shahbaz et al. 1999). We discuss this in more detail in Sect. 4.1.

#### 4. Using least-squares deconvolution

Ideally what we would like to do is observe a single high signal-to-noise isolated absorption line, from which we can directly measure the shape of the line profile. The Least-Squares Deconvolution (LSD) method (Donati et al. 1997) allows us to do exactly this. LSD is a cross-correlation technique that effectively stacks the thousands of stellar absorption lines in an echelle spectrum to produce a single “average” absorption line profile with increased signal-to-noise ratio; theoretically the increase in signal-to-noise ratio is the square root of the number of lines observed. It has been used in the spectropolarimetric observations of active stars (Donati et al. 1997) and in Doppler imaging studies (e.g. see Barnes et al. 2004). More recently, LSD has been used in conjunction with Roche-tomography to map the surface distribution of the secondary stars in cataclysmic variables (e.g. Watson et al. 2006). With LSD we obtain a single high-quality line profile from which we can readily determine the rotational broadening.

LSD assumes that all the absorption lines are rotationally broadened by the same amount, and hence just requires the position and strength of the observed lines in the echelle spectrum to be known. We generated a line list appropriate for a K0 III star from the Vienna Atomic Line database (Kupka et al. 1999, 2000). Approximately 3100 lines were used in the deconvolution process across both the red and green spectra. Our version of LSD propagates the errors through the deconvolution process.

LSD profiles were computed for the individual flux calibrated V395 Car and K0 III star spectra. The LSD profiles of V395 Car were then averaged and compared to the rotationally broadened version of the template star LSD profile using the optimal subtraction procedure. Basically, we repeat the standard method described earlier, but this time using the LSD profiles of the green and blue spectra which only contain a single absorption line (see Fig. 4). We obtain  $v \sin i$  values of  $31.3 \pm 0.5 \text{ km s}^{-1}$  and  $34.7 \pm 0.5 \text{ km s}^{-1}$  using zero and continuum limb-darkening respectively for the combined green and red LSD profiles (minimum reduced  $\chi^2$  of 0.90 and 0.97 and respectively). Although these values agree well with what we obtained in Sect. 3, there are less systematic uncertainties in the analysis of the LSD line

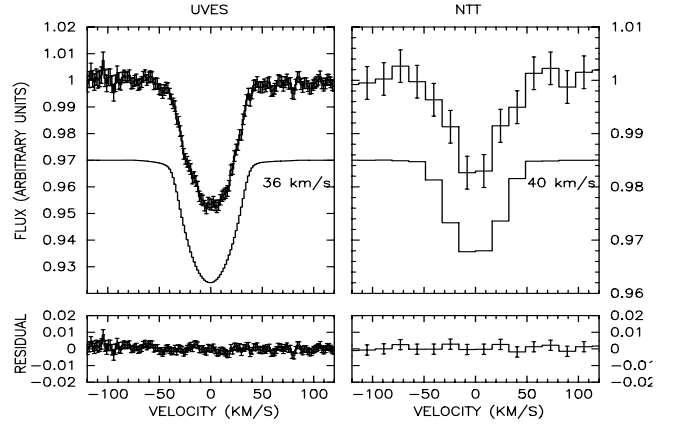


**Fig. 4.** The results of the  $v \sin i$  analysis using LSD profiles. The uppermost plot shows the LSD profile determined from the green and red spectra of V395 Car. The LSD profile below (offset for clarity) shows the LSD profile of the K0 III template star rotationally broadened using a continuum limb-darkened spherical rotation profile and scaled to match the top profile. The bottom panel shows the residual after the optimal subtraction. The left and right panels show the results for the UVES and NTT data respectively.

profiles, primarily because one can clearly discern the shape of the high signal-to-noise absorption line profile (see Sect. 4.1).

We can now use the determined  $v \sin i$  (assuming limb-darkening) and optimally subtract the broadened template spectra from the V395 Car and determine the fractional contribution of the K0 III secondary star to the total flux. We obtain  $0.26 \pm 0.02$ ,  $0.30 \pm 0.01$  and  $0.33 \pm 0.01$  for the blue, green and red spectra respectively.

##### 4.1. Re-analysis of the NTT data using LSD

The data published in Shahbaz et al. (1999) was taken with the NTT+EMMI and has a  $FWHM$  resolution of  $0.83 \text{ \AA}$  ( $=38.3 \text{ km s}^{-1}$ ). Our analysis of the data revealed a  $v \sin i$  of  $64 \pm 9 \text{ km s}^{-1}$ . (It should be noted that the template star used in the analysis of the NTT data of V395 Car was actually taken at the WHT in 1992 (Casares & Charles 1994) and had a resolution of  $0.5 \text{ \AA}$ , better than the NTT data.) In an attempt to understand why the NTT data gives a higher value for the secondary star’s rotational broadening, we computed the LSD profile of the average spectrum presented in Shahbaz et al. (1999). We then performed the standard  $v \sin i$  analysis and optimal subtraction, using the LSD profile of the UVES K0 III star degraded to match the resolution of the NTT data. Using the appropriate continuum limb-darkening coefficient (as in Shahbaz et al. 1999), we obtain a  $v \sin i$  of  $40 \pm 10 \text{ km s}^{-1}$ , consistent with the value we obtained using the UVES data (see Fig. 4). Note that a  $v \sin i$  of  $40 \text{ km s}^{-1}$  corresponds to a rotational profile with an equivalent  $FWHM$  of  $60.6 \text{ km s}^{-1}$ , which is only a factor of 1.6 more than the instrumental resolution.

This difference is most likely due to a combination of the low signal-to-noise and resolution of the NTT data, which results in the broad absorption blend near  $6495 \text{ \AA}$  dominating the  $\chi^2$  of the comparison between the target spectrum and the scaled rotationally broadened template star spectrum. We tested this hypothesis by performing our original analysis (as was done in Shahbaz et al. 1999) but masking the broad  $6495 \text{ \AA}$  blend. Indeed we find that we obtain a  $v \sin i$  of  $41 \pm 15 \text{ km s}^{-1}$  compared to  $64 \pm 9 \text{ km s}^{-1}$  when using all the features, suggesting that the

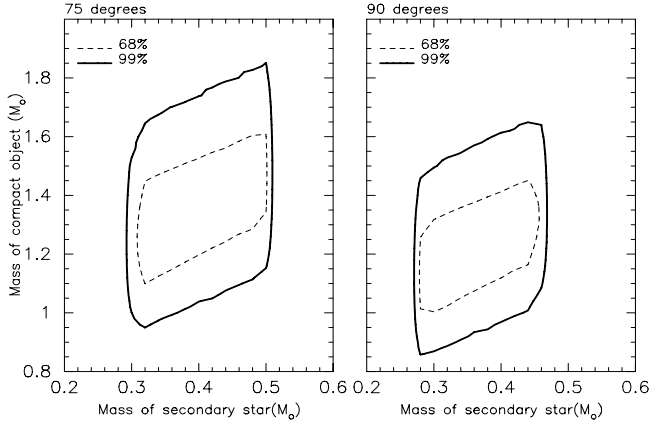


**Fig. 5.** The mass of the binary components obtained using a Monte Carlo simulation (see Sect. 5). The solid and dashed lines show the 99% and 68% confidence levels respectively. The left and right panels are for binary inclination angles of  $75^\circ$  and  $90^\circ$  respectively.

6495 Å blend adds a systematic uncertainty in the determination of  $v \sin i$  when using low-resolution low signal-to-noise data. We thus encourage the use of LSD as a secondary check on the  $v \sin i$  measurements in order to avoid such systematics from passing by unnoticed.

## 5. The system parameters

Since the companion star fills its Roche lobe, *assuming it is* synchronized with the binary motion, the rotational broadening provides a direct measurement of the binary mass ratio,  $q (=M_2/M_1$ :  $M_1$  and  $M_2$  are the mass of the compact object and secondary star respectively), through the expression  $v \sin i = K_2(1+q)R_2/a$  (Horne et al. 1986), where  $K_2$ ,  $R_2$  and  $a$  are the secondary star’s radial velocity semi-amplitude, radius and the binary separation, respectively. Therefore, substituting the values for  $K_2$  (Shahbaz et al. 2004) and  $v \sin i$  we find  $q = 0.281 \pm 0.034$ . Furthermore, using  $K_2$  and  $q$ , with the orbital period  $P_{\text{orb}}$  and the binary inclination  $i$ , we can determine the masses of the compact object,  $M_1$ , and the companion star,  $M_2$ , using the mass function  $PK_2^3/2\pi G = M_1 \sin^3 i/(1+q)^2$ . In order to determine the uncertainties in  $q$ ,  $M_1$  and  $M_2$  we used a Monte Carlo simulation, in which we draw random values for the observed quantities which follow a given distribution, with mean and variance the same as the observed values. For  $K_2$  the distribution is taken to be Gaussian as the uncertainty is symmetric about the mean value. However for  $v \sin i$  we take a uniform random distribution, because of the uncertainties in the limb-darkening;  $31.3\text{--}2.33\sigma$   $\text{km s}^{-1}$  to  $34.7 + 2.33\sigma$   $\text{km s}^{-1}$  (99% confidence).

Given the measured masses and orbital period, we use Kepler’s Third Law to determine the semi-major axis  $a$ . Eggleton’s expression for the effective radius of the Roche-lobe (Eggleton 1983) then determines the radius of the secondary  $R_2$ , the temperature (4800 K) is inferred from the spectral type (Gray 1992) and finally Stefan-Boltzmann’s law determines the luminosity  $L_\odot$ . Figure 5 shows the allowed mass range for the binary components for the limits on the inclination angles of  $75^\circ$  and  $90^\circ$  (Shahbaz et al. 2004), and Table 2 gives the determined system parameters. Similar results have also been recently obtained by Steeghs & Jonker (2007).

**Table 2.** Summary of derived system parameters. The uncertainty in the binary masses are  $1\text{-}\sigma$  and the others are at the 99% confidence level.

Parameter	$i = 75^\circ$	$i = 90^\circ$
$M_1 (M_\odot)$	$1.37 \pm 0.13$	$1.23 \pm 0.12$
$M_2 (M_\odot)$	0.30–0.49	0.27–0.45
$R_2 (R_\odot)$	5.56–6.61	5.37–6.39
$L_2 (L_\odot)$	14.5–23.3	13.6–19.2
$a (R_\odot)$	20.0–20.5	19.2–22.5

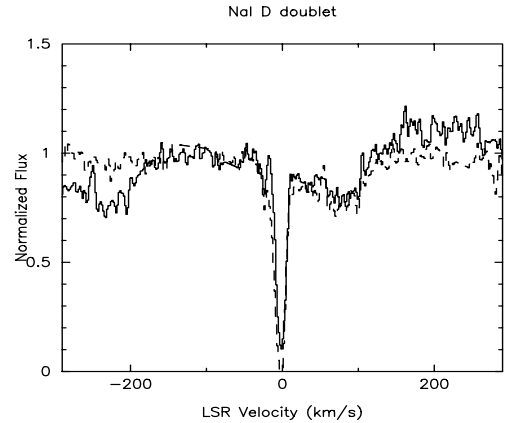


**Fig. 6.** The Na I D1 (5895.92 Å) and D2 (5889.95 Å) doublet converted to the frame of the local standard at rest (LSR). The solid and dashed lines are the D1 and D2 components respectively.

## 6. Interstellar reddening

We clearly detect the Na I D interstellar lines in absorption which, although very deep, are not saturated (see Fig. 6). The equivalent width ( $EW$ ) of the Na I D1 (5895.92 Å) and D2 (5889.95 Å) components were measured to be  $0.56 \pm 0.02$  Å and  $0.74 \pm 0.02$  Å respectively. Note that the He I feature at 5875.62 Å is not broad and so does not contaminate the Na I D1 feature (see Fig. 2). The ratio between the two Na lines is much less than the factor of two expected at the lowest optical depths (Munari & Zwitter 1997). Using the empirical relationship of Barbon et al. (1990) the total  $EW$  of the doublet corresponds to  $E(B - V) = 0.33 \pm 0.01$  mag. For comparison, the hydrogen column as estimated from the Schlegel dust maps (Schlegel et al. 1998) gives  $E(B - V) = 0.25$  mag, whereas the hydrogen column estimated from the HI maps of Dickey & Lockman (1990) gives  $E(B - V) = 0.31$  mags ( $N_{\text{H}} = 1.69 \times 10^{21}$  atoms  $\text{cm}^{-2}$ ) assuming  $E(B - V) = A_{\text{V}}/3.1$ ; and  $N_{\text{H}} = 1.79 \times 10^{21} A_{\text{V}}$  atoms  $\text{cm}^{-2}$  (Rieke & Lebofsky 1985; Predehl & Schmitt 1995).

## 7. Discussion

Comparing V395 Car with Cyg X–2 one notes some very interesting similarities. Both systems are long period binaries in the halo of the Galaxy, they are at high inclination angles with evolved secondaries and have similar binary mass ratios,  $q = 0.34$  (Casares et al. 1998) and  $q = 0.281$  (Sect. 5) for Cyg X–2 and V395 Car respectively. Cyg X–2 is known to contain a neutron star because type I X-ray bursts are observed (Kahn & Grindlay 1984). Although no bursts or pulsations have been seen in V395 Car, our mass determination implies that it contains a neutron star (Sect. 5). However, it should be noted that the secondary star in V395 Car is much cooler (K0 III) and hence less luminous than the secondary star in Cyg X–2 (A9 III; Casares et al. 1998), contrary to what we might have expected

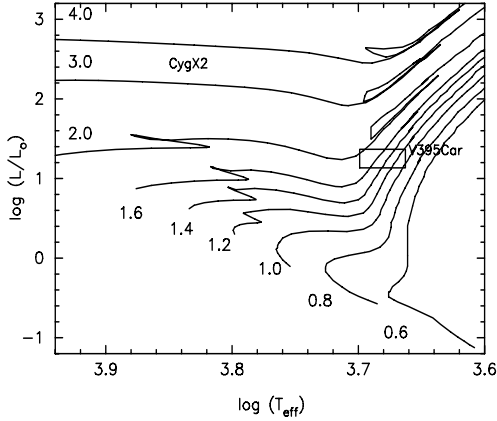


**Fig. 7.** Hertzsprung-Russell diagram with evolutionary tracks for solar metallicity stars in the range  $0.6\text{--}3.0 M_{\odot}$  (Girardi et al. 2000). The box shows the position of the observed effective temperature ( $4800 \pm 200$  K) and luminosity of the secondary star in V395 Car (see Table 2). We also show the position of Cyg X–2 which despite having similar system parameters, has a very different evolutionary history compared to V395 Car.

given their inferred masses. This difference is related to the very different evolutionary histories. The secondary star in Cyg X–2 started to transfer mass near the end of its main-sequence phase (Case AB; Podsiadlowski & Rappaport 2000). Most of the mass of the secondary was ejected from the system during an earlier rapid mass transfer phase and currently we observe the hot inner core of what had been initially a more massive star.

We can compare the mass and radius of a normal K0 III star ( $M_2 = 2.3 M_{\odot}$ ;  $R_2 = 11 R_{\odot}$ ; Gray 1992) to the observed values of V395 Car of  $M_2 \sim 0.4 M_{\odot}$  and  $R_2 \sim 6 R_{\odot}$ . The observed values suggest that the secondary star in V395 Car is more evolved and has a lower mass compared to a normal K0 III star. Placing the observed secondary star on the Hertzsprung-Russell diagram we find that its position corresponds to a normal single star with mass  $0.6\text{--}1.4 M_{\odot}$  that has crossed the Hertzsprung gap and now lies on the Hayashi line. The evolution of the binary is dominated by the evolution of the evolved secondary star and the mass transfer is early massive Case B, because such a star no longer burns hydrogen in its core (Case A can be ruled out because the observed secondary star does not resemble a single star of the same mass). For a binary with a secondary star near the onset of such mass transfer, one requires  $q < 1$  throughout its history (King & Ritter 1999). The position of a secondary on the Hertzsprung-Russell diagram undergoing early massive Case B mass transfer is close to that of a single star of the same mass. For a  $1.4 M_{\odot}$  compact object this implies  $M_2 < 1.4 M_{\odot}$ , which is consistent with the single star mass corresponding to the observed properties of the secondary star.

## 8. Conclusions

We have accurately measured the rotational broadening ( $v \sin i$ ) in V395 Car using UVES echelle spectroscopy and the method

of Least-Squares Deconvolution (LSD), which provides a single high signal-to-noise ratio absorption line profile. We determine  $v \sin i$  to be  $31.3 \pm 0.5 \text{ km s}^{-1}$  to  $34.7 \pm 0.5 \text{ km s}^{-1}$  (assuming zero and continuum limb darkening, respectively). The disagreement with previous results is most likely due to a combination of low signal-to-noise ratio and the relatively low spectral resolution of the data. We find that using relatively low-resolution spectroscopy can result in systemic uncertainties in the measured  $v \sin i$  values obtained using standard methods. We suggest the use of LSD as a secondary, reliable check of the results because LSD allows one to directly discern the shape of the absorption line profile. Using our revised  $v \sin i$  value in combination with the secondary star’s radial velocity gives a binary mass ratio of  $0.281 \pm 0.034$ . Furthermore, assuming a binary inclination angle of  $75^{\circ}$  gives a compact object mass of  $1.37 \pm 0.13 M_{\odot}$ , consistent with a canonical neutron star mass.

*Acknowledgements.* T.S. acknowledges support from the Spanish Ministry of Science and Technology under the programme Ramón y Cajal. C.A.W. is supported by a PPARC postdoctoral fellowship.

## References

- Barbon, R., Benetti, S., Rosino, L., Cappellaro, E., & Turatto, M. 1990, *A&A*, 237, 79
- Barnes, J. R., James, D. J., & Cameron, A. C. 2004, *MNRAS*, 352, 589
- Branduardi-Raymont, G., Corbet, R. H. D., Mason, K. O., et al. 1983, *MNRAS*, 205, 403
- Casares, J., & Charles, P. A. 1994, *MNRAS*, 271, L5
- Casares, J., Charles, P. A., & Kuulkers, E. 1998, *ApJ*, 493, L39
- Chevalier, C., & Ilovaisky, S. A. 1981, *A&A*, 94, L3
- Collins, G. W., II, & Truax, R. J. 1995, *ApJ*, 439, 860
- Dickey, J. M., & Lockman, F. J. 1990, *ARA&A*, 28, 215
- Donati, J.-F., Semel, M., Carter, B. D., Rees, D. E., & Collier Cameron, A. 1997, *MNRAS*, 291, 658
- Eggleton, P. P. 1983, *ApJ*, 268, 368
- Girardi, L., Bressan, A., Bertelli, G., & Chiosi, C. 2000, *A&AS*, 141, 371
- Gray, D. F. 1992, *Cambridge Astrophysics Series* (Cambridge: Cambridge University Press), 2nd edn.
- Horne, K., Wade, R. A., & Szkody, P. 1986, *MNRAS*, 219, 791
- Jonker, P. G., Steeghs, D., Nelemans, G., & van der Klis, M. 2005, *MNRAS*, 356, 621
- Kahn, S. M., & Grindlay, J. E. 1984, *ApJ*, 281, 826
- King, A. R., & Ritter, H. 1999, *MNRAS*, 309, 253
- Kupka, F., Piskunov, N., Ryabchikova, T. A., Stempels, H. C., & Weiss, W. W. 1999, *A&AS*, 138, 119
- Kupka, F. G., Ryabchikova, T. A., Piskunov, N. E., Stempels, H. C., & Weiss, W. W. 2000, *Balt. Astron.*, 9, 590
- Li, F. K., Clark, G. W., Jernigan, J. G., et al. 1978, *Nature*, 276, 799
- Marsh, T. R., Robinson, E. L., & Wood, J. H. 1994, *MNRAS*, 266, 137
- Mason, K. O., Branduardi-Raymont, G., Codova, F. A., & Corbet, R. H. D. 1987, *MNRAS*, 226, 423
- Munari, U., & Zwitter, T. 1997, *A&A*, 318, 269
- Podsiadlowski, P., & Rappaport, S. 2000, *ApJ*, 529, 946
- Predehl, P., & Schmitt, J. H. M. M. 1995, *A&A*, 293, 889
- Rieke, G. H., & Lebofsky, M. J. 1985, *ApJ*, 288, 618
- Schlegel, D. J., Finkbeiner, D. P., & Davis, M. 1998, *ApJ*, 500, 525
- Shahbaz, T. 2003, *MNRAS*, 339, 1031
- Shahbaz, T., Kuulkers, E., Charles, P. A., et al. 1999, *A&A*, 344, 101
- Shahbaz, T., Casares, J., Watson, C. A., et al. 2004, *ApJ*, 616, L123
- Steenhals, D., & Jonker, P., 2007, *ApJ*, submitted, <http://arxiv.org/abs/0707.2067>
- Watson, C. A., Dhillion, V. S., & Shahbaz, T. 2006, *MNRAS*, 368, 637